SOFT ROBOTICS
Volume 00, Number 00, 2023

DOI: 10.1089/soro.2022.0118

SoRo
Soft Robotics

Squid-Inspired Powerful Untethered Soft Pumps via Magnetically Induced Phase Transitions

Qin Jiang, Zhitong Hu, Kefan Wu,* Wenjun Wu, Shuo Zhang, Han Ding, and Zhigang Wu

Abstract

Soft robots possess unique deformability and hence result in great adaptability to various unconstructive environments; meanwhile, untethered soft actuation techniques are critical in fully exploiting their potential for practical applications. However, restricted by the material's softness and structural compliance, most untethered actuation systems were incapable of achieving fully soft construction with a powerful output. While in Nature, with a fully soft body, a squid can burst high-pressure jet flow from a cavity that drives the squid to swim swiftly. Here, inspired by such a unique actuation strategy of squids, an entirely soft pump capable of high-pressure output, fast jetting, and untethered control is presented, and it helps a bionic soft robotic squid to achieve a high-efficient untethered motion in water. The soft pump is designed by a reversible liquid–gas phase transition of an inductive heating magnetic liquid metal composite that acts as an adjustable power source with high heat efficiency. In particular, being purely soft, the pump can yet lift $\sim$20 times its weight and achieve $\sim$3 times the specific pressure of the previous record. It may promote the application of soft robots with independent actuation, high output power, and embodied energy supply.

Keywords: untethered soft pump, magnetic liquid metal composite, tunable magnetic susceptibility, phase transition, bioinspired

Introduction

Possessing excellent deformability, compliance, and interactivity, soft robots have been well developed with novel constructions and functionalities for utilizing in unconstructive/unpredictable scenarios, for example, multi-item grabbing,[1–3] invasive surgery,[4,5] narrow space drag delivery,[6–8] and human–machine interface.[9,10] Among soft robot's construction, an actuation system has been playing a core role in achieving controllable locomotion and thus precise assignment operation. Tethered soft actuation systems, for example, pneumatic and hydraulic ones,[11] are the most widely used to provide enough drive power. Nevertheless, the wire also limits many promising application scenarios for soft robots, for example, uncharted enclosed territory exploration and wide-range mission execution. Thus, untethered soft actuation techniques are urgently needed to realize automatic and untethered soft robotic systems, particularly for highly interactive and unconstructive scenarios.[12]

State Key Laboratory of Digital Manufacturing Equipment and Technology, School of Mechanical Science and Engineering, Huazhong University of Science and Technology, Wuhan, China.
Current affiliation: College of Engineering, Northeastern University, Boston, Massachusetts, USA.

Previously, various untethered soft actuation techniques have been proposed, including pneumatic inflation,[13–15] dielectric elastomer actuator (DEA),[16,17] electrohydrodynamic (EHD),[18] magnetic,[19,20] light,[21] phase transition,[22,23] etc. However, they either suffer from (1) nearly most of them, severely rely on bulk onboard components, for example, mechanical pumps,[14,24,25] gas tanks,[13,15] rigid architectures,[22,23] and electrical hardware,[16–18] that cannot be fully integrated into soft robots' body and thus influence their integral deformability; or (2) some of them, fully soft untethered actuators that are derived by external stimuli fields, for example, magnetic field[26–28] and light,[29–31] can be integrated into small-size soft robots, but these actuators cannot provide sufficient high power, which is compromised by the materials' softness and structural compliance. Hence, developing an actuation system possessing soft, powerful, and untethered control simultaneously is still technically challenging at the current stage.

While in Nature, aquatic invertebrates with soft structures provide characteristic solutions. Squids develop a unique locomotion system to stealthy and swiftly swim and reach the fastest speed (~ 8 m/s)[32] known among aquatic invertebrates. Inside the highly deformable body, a soft mental cavity filled with fluid can repeatedly expand and contract to burst pulse-jet water for swimming and spraying ink in danger (Fig. 1a). Thus, squids can realize high propulsive efficiency by precisely directly housing the energy source within their bodies. Several squid-inspired robots have been demonstrated by imitating the squid's pulse-jet behavior; however, they still rely on rigid mechanical systems.[33,34] Meanwhile, the phase-change soft actuation technique utilizing inductive heating technology of nanoparticles can provide high power-density output.[22] However, its long actuation response time (over 130 s) strictly limits its application in soft robots due to the low heating efficiency of nanoparticles.

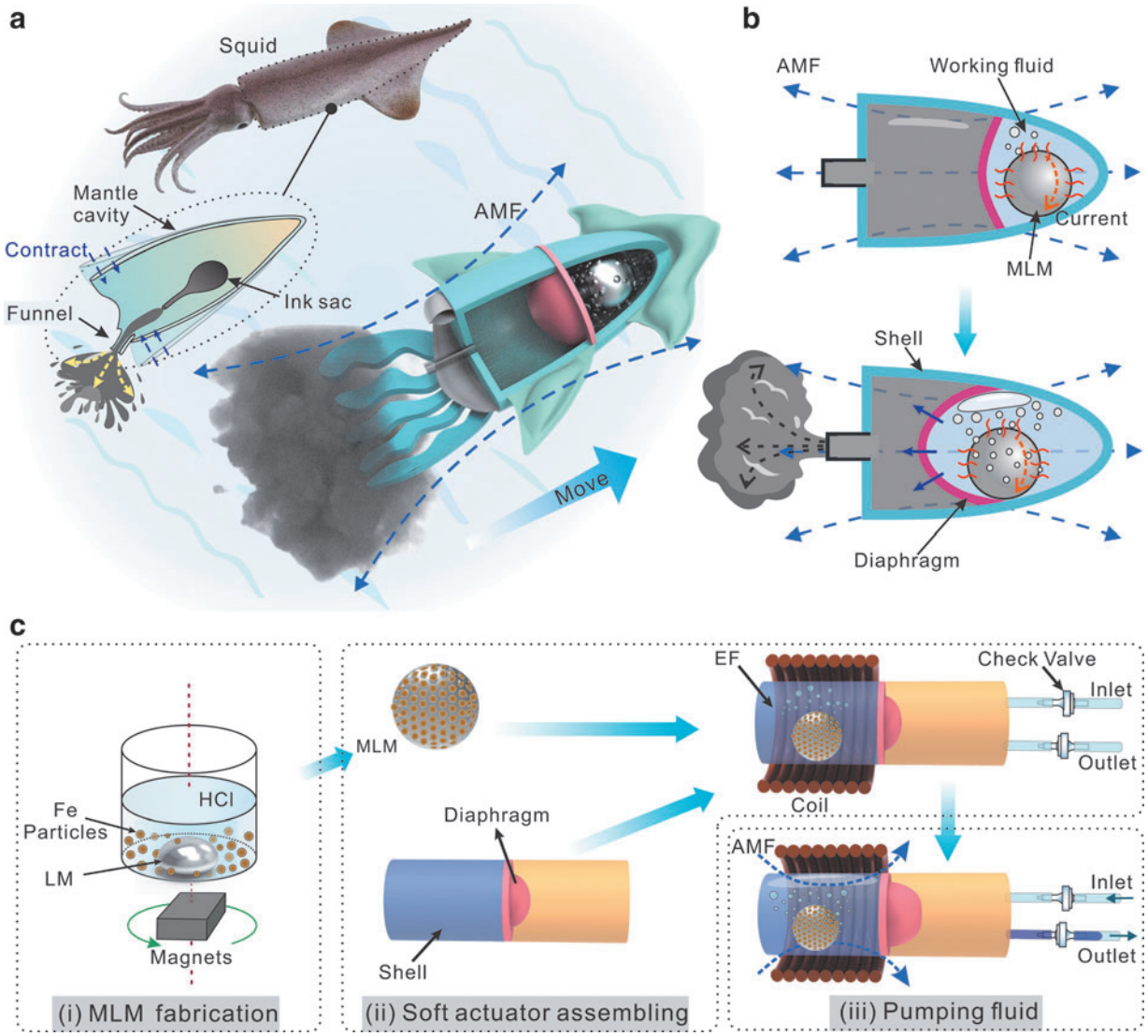

FIG. 1. Bio-inspiration, actuation mechanism, and fabrication of ECSDP. **(a)** A squid contracting mantle cavity to jet ink and a squid-like robot. **(b)** Sectional illustrations of the squid-like soft robot. *Upper*: the eddy current in the MLM generates the heat by the AMF induction. *Below*: the soft diaphragm expands under the high pressure of the head chamber and jets the black ink. **(c)** Brief fabrication process of the cylindrical ECSDP. AMF, alternating magnetic field; ECSDP, electromagnetic-controlled soft diaphragm pump; LM, liquid metal; MLM, magnetic liquid metal.

Recently, liquid metal (LM; e.g., Gallium-based alloy) has been widely employed in soft robots as the heat-generating source,[35,36] owing to its high electric conductivity,[37,38] high thermal conductivity,[39,40] and super compliant deformability.[41–43] Moreover, magnetic liquid metal (MLM) composites can reach a relatively high inductive heating speed due to their high magnetism.[44] However, the relationship between the heating speed and the magnetic susceptibility of the composite was not well explored.

In this work, inspired by the unique actuating construction of squids, we propose an electromagnetic-controlled soft diaphragm pump (ECSDP) for soft robots, which is fully soft, high-pressure output drove, untethered controlled, and suitable for pumping various fluidic media. The ECSDP can be embedded into a squid-mimicking soft robot, enabling the biomimetic squid to swim in the water freely by strongly jetting black ink. The soft squid robot has a completely soft body with two chambers, separated by a rubber diaphragm (Fig. 1b). A MLM sphere is placed into the head chamber as the heat source. Induced by an alternating magnetic field (AMF), the eddy current in the MLM sphere generates heat to the working fluid, causing fluid gasification and thus raising the pressure inside the chamber. As the diaphragm has a lower rigidity than that of the shell, it expands by the high-pressure gas of the head chamber and jets the ink out from the tail.

Materials and Methods

Fabrication of cylindrical ECSDP

The cylindrical ECSDP consists of three basic components: an MLM sphere, a soft body, and two check valves. The fabrication process can be summarized into three major processes: (1) MLM fabrication, (2) soft body molding, and (3) soft pump assembling (details in Supplementary Fig. S1). The dimensions of the cylindrical ECSDP can be found in Supplementary Figure S2a.

Fabrication of soft robotic squid

A large-sized MLM sphere ($\sim$20 mm diameter and $\sim$10 g weight) was placed in the head chamber to provide enough actuating power. Four soft rubber airbags (Ecoflex 00-10) were bonded with the soft body to provide suitable buoyancy (Supplementary Fig. S2b).

Characterizations

Magnetic hysteresis loops of various samples (MLM and Fe particles) were tested using a superconducting quantum interference device at 298K (SQUID-VSM 0-7T; Quantum Design, USA). The surface temperature change of the samples was recorded using a thermal camera (T640; Flir, USA) (details in Supplementary Fig. S3). The temperature and pressure change of the working fluid (Novec 7000; 3M, USA) was tested using a thermometer (DM6801A; LIHUADA, China) and a manometer (GM510; BENETECH, China), respectively. The 5 mL of working fluid and an 8 mm diameter MLM sphere were placed into a glass bottle and heated by an AMF. As the resistive probe of the thermometer could also be heated by the AMF, the stable temperature data were selected at 1s after stopping the remote heat.

The measurement process of various fluidic media's flow rates is in Supplementary Figure S4. The bending stiffness of the soft diaphragm was calculated by $Et^3/12(1-v^2)$, where E is Young's modulus, t is the thickness, and v is the Poisson ratio of the Ecoflex 00-10. The E is 37 kPa, and v is 0.49.[45] The details of the working pressure measurement of the cylindrical ECSDP can be found in Supplementary Figure S5.

Induction heating apparatus

The cylindrical ECSDP was inductively heated by a 180 kHz mini zero voltage switching suite (ZVS), which can adjust the excitation power (0–48 W) by changing the input voltage. The soft robotic squid was heated by a power of 1 kW ZVS with a magnetic frequency of 70 kHz.

Finite element analysis

The simulation results were solved by COMSOL 5.6a. The Yeoh hyperelastic model was selected to simulate the incompressible silicone rubber (Ecoflex 00-10).

Results and Discussion

ESCDP fabrication

To facilitate the measurement of the ESCDP characteristics, we configure the ESCDP into a cylindrical shape (Fig. 1c). First, the MLM was obtained by compositing LM and iron (Fe) particles in concentrated hydrochloric acid. Then, the ECSDP was assembled by a formability MLM sphere, soft rubber shell with the diaphragm, and working fluid (Novec 7000, which is safe and low toxicity). All-soft-matter architectures enable the pump to be fully soft (Supplementary Fig. S6a). After that, two check valves were connected to the soft pump to regulate the flow direction. Finally, the ECSDP could pump in and out the fluid under the control of AMF (Supplementary Fig. S6b).

Tunable heat power of MLM and working principle of ECSDP

As the core heating component of the ECSDP, MLM transferred the external energy of electromagnetic to gasify the working fluid. Thus, speeding up the heat generation of MLM is vital to accelerate the response time of the ECSDP. To investigate the heating mechanism of MLM, we prepared various weight ratios (wt%) of Fe particles in MLM samples and measured the corresponding fluidity (Fig. 2a). With increasing mixing ratio, the MLM gradually transforms from fluid (0 wt%, pure LM) to solid-like paste (40 wt% of Fe), easily shaping into a sphere with good plasticity. However, when the weight ratio is close to 50 wt%, the MLM separates into individual particles with a diameter of $\sim$2 mm.

To investigate Fe particles' influence on the heat power of composites, we conducted a series of experiments. As in Figure 2b, the magnetic hysteresis loops of various wt% MLM and Fe particles were tested. The magnetic susceptibility (χ_m, the slope of the magnetic hysteresis loop) of pure LM is nearly zero, indicating the nonmagnetic property of pure LM. With the doping ratio of Fe particles gradually increasing, the χ_m of various composite samples (10–50 wt%) gradually increases and tends to saturation at 50 wt%. Moreover, the induction heating rate of MLM samples with various weight ratios was investigated (Fig. 2c). With the weight ratio of Fe increasing from 0 to 40 wt% on the

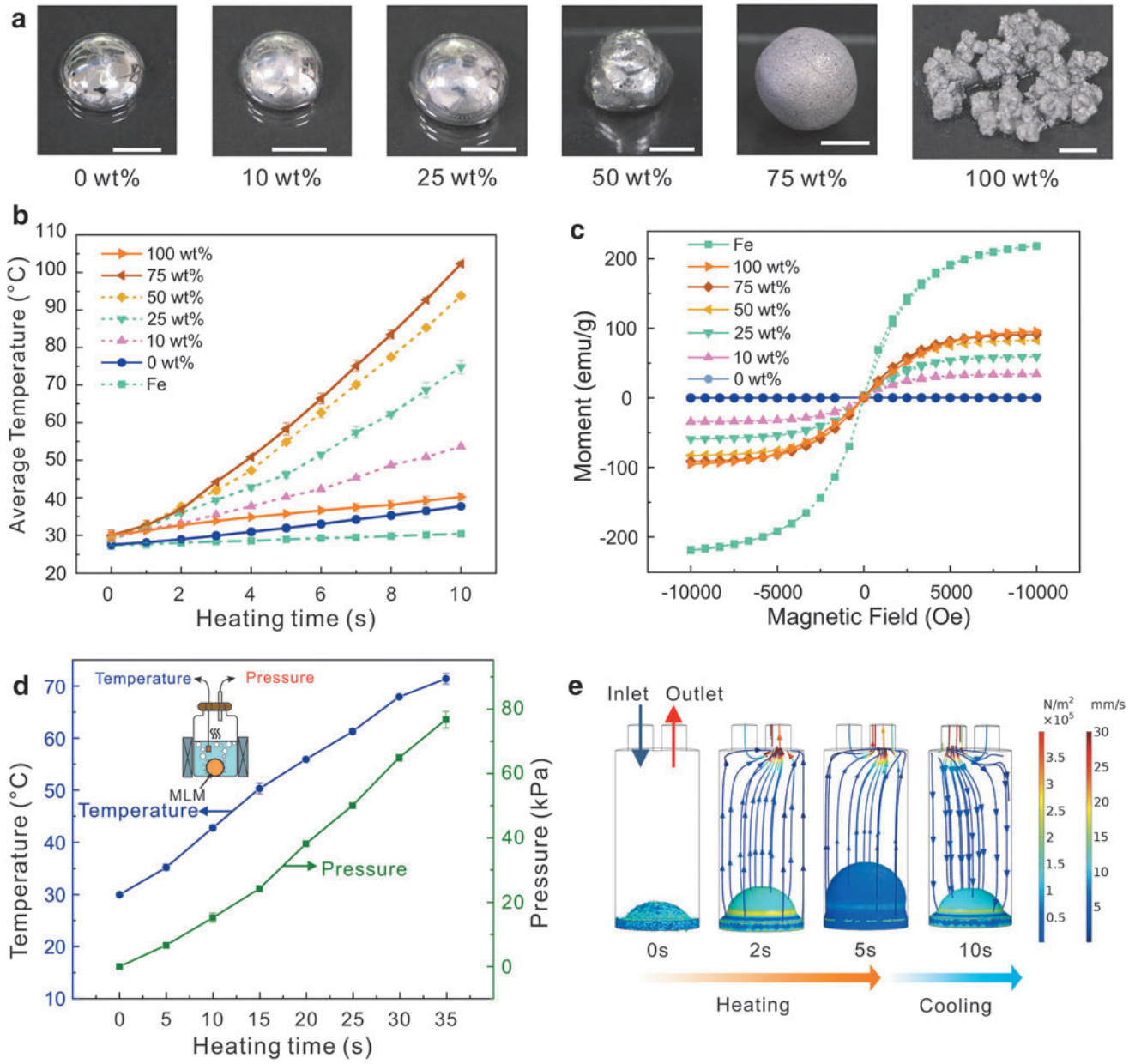

FIG. 2. Tunable heat power of MLM and working principle of ECSDP. **(a)** Photos of the MLM samples from 0 to 50 wt%. wt%, the ratio of Fe particles mass to the total mass in MLM. 0 wt%, the pure LM without Fe particles mixing. Scale bars = 5 mm. **(b)** Magnetic hysteresis loop of MLM with various mass ratios and Fe particles at 298 K. **(c)** Surface average temperature of MLM samples with various mass ratios and Fe particles in inductively heating. The current of the spiral coil is set as 24 A. **(d)** Temperature and pressure curves of the working fluid heated by MLM. **(e)** Simulated result of pumping fluid process during heating and cooling conditions in 10 s.

condition of an 8 mm diameter of the MLM, the heating speed of composites gradually increases. Notably, the temperature of the 40 wt% composite increases from 30°C to 102.3°C (72.3°C increase), which is about 7 times faster than that of the pure LM (0 wt%, 10.2°C increase) within the same heating time (10 s).

According to the analytical model $P \propto [1+\chi_m]^2$, the heating power of magnetic composites is positively correlated with their magnetic susceptibility (χ_m) under the same diameter (details in Supplementary Note 1), which is consistent with our experiments with inductive heating. Although the χ_m of 50 wt% MLM and Fe particles are desirable, their separated tiny particles (diameters of 2 mm and 50 nm, respectively) decrease the heating power, which in turn results in the temperature increasing speed of the 50 wt% MLM being lower than that of 10 wt%, and Fe particles' temperature only increases slightly. Based on the above analysis, we selected the 40 wt% MLM as the heating source of our soft pump due to its superb heating speed yet preferable plasticity.

The pressure changes of working fluid during the liquid–gas phase transition are also investigated (Fig. 2d). The working fluid was positioned in a glass bottle and heated by a

40 wt% MLM sphere. After 5 s of heating, the working fluid's temperature increased from 30°C to 35°C and began to boil. The pressure inside the bottle also raised rapidly from 0 to ~6.5 kPa by the inflation of working fluid vaporization. Then, the temperature and pressure increased on the continuous heating, indicating that the working fluid can provide huge actuating pressure.

We also conduct a numerical approach to simulate the pumping process of the cylindrical ECSDP under heating and cooling conditions (Fig. 2f). During the heating process (the

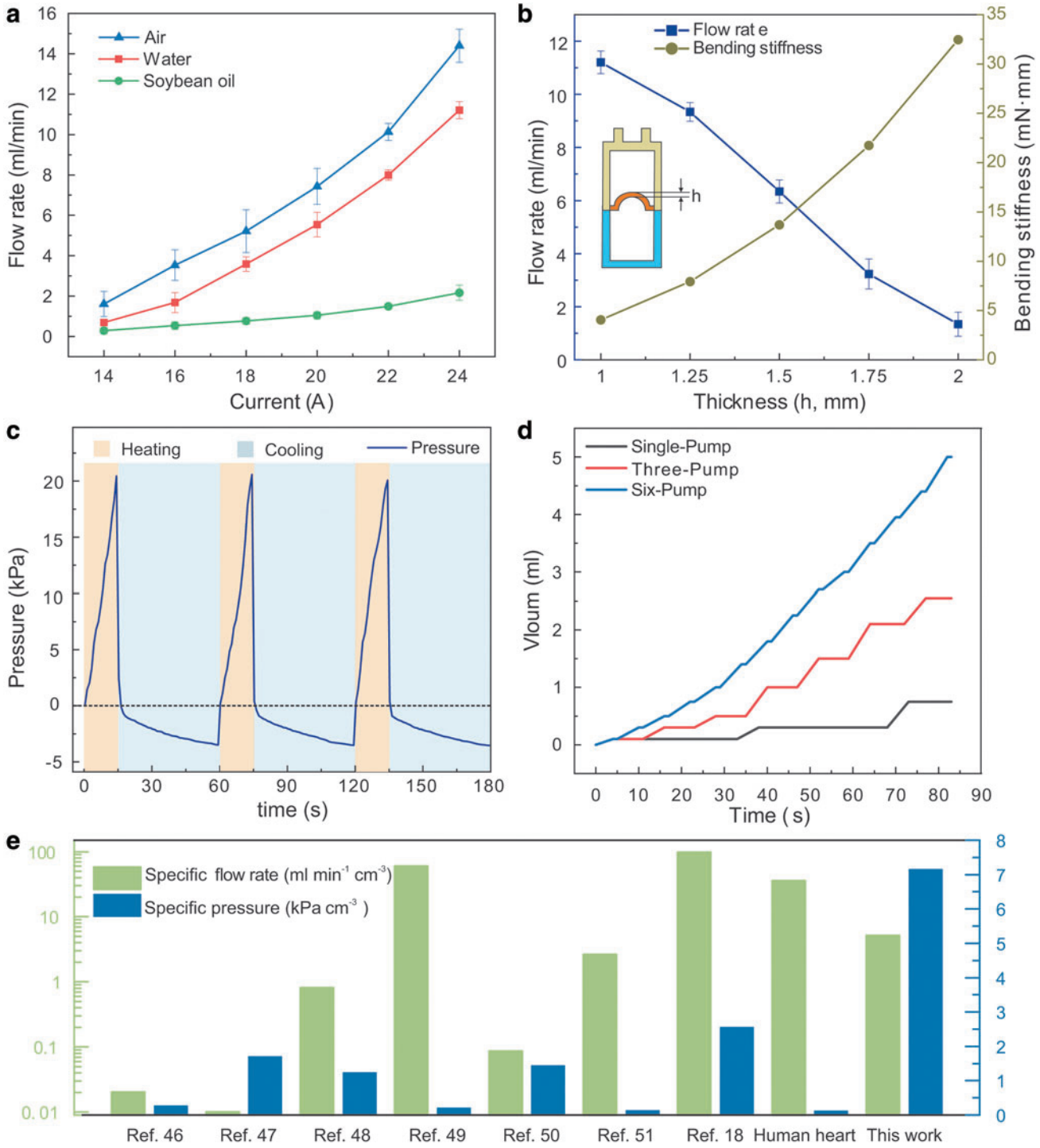

FIG. 3. Actuation characterization of the soft pump. **(a)** Flow rate change of various media at different currents on the spiral coil. **(b)** Water flow rate and bending stiffness of diaphragm with different thicknesses (h). The coil current was set at 24 A. **(c)** Pumping pressure with time curve under heating and cooling cycling. **(d)** Pumping out the volume of water with time curves under single, triple, and six-pump groups. **(e)** Performance comparison between the ECSDP, soft pumps, and human heart.

first 5 s), the soft diaphragm gradually expands and thus forces the fluid out under a pressure of 6.5 kPa. During the cooling process, the soft diaphragm retracted under its own resilience, drawing the fluid into the chamber from the inlet; therefore, periodical pumping can be realized by cycling the heating and cooling conditions. The simulation result of the diaphragm's deformation is consistent with the experiment result (Supplementary Fig. S7), proving the rationality of the design.

Pumping characterization

The ECSDP can pump various fluidic media, for example, air, water, and soybean oil, and the flow rate of various fluids can be controlled by adjusting the electric current on the spiral coil (Fig. 3a). With the current gradually increasing, the thermal energy of the MLM is improved (details in Supplementary Note 1). Thus, the soft diaphragm was expedited to expansion under the rapid gasification of the working fluid, causing the flow rate of the three media to increase. In addition, the result indicates that the outflow rate of air is the highest (14.4 mL/min), whereas the outflow rate of soybean oil is the lowest (2.2 mL/min) of the three media at the same current of 24 A. The difference in their outflow rate depends on the viscous resistance of the tube and valve. As the dynamic viscosity of air (1.8×10^{-5} Pa/s), water (1×10^{-3} Pa/s), and soybean oil (47.9 Pa/s) gradually increases at 20°C, the viscous resistance of substances becomes greater when they were pumped. Theoretically, the result indicates that the ECSDP can pump various fluidic media in a wide viscosity range (1.8×10^{-5} to 47.9 Pa/s), which can cross a scale over one million.

As shown in Figure 3b, the pumping flow rate is associated with the thickness (h) of the soft diaphragm. As the thickness increases from 1 to 2 mm, the water flow rate decreases from 11.2 to 1.3 mL/min, whereas the bending stiffness of the diaphragm increases from 4.1 to 32.5 mN m. The result indicates that a thinner diaphragm can achieve a higher flow rate than a thicker diaphragm due to its lower stiffness. However, our experiment found that extremely thin diaphragms (<1 mm) cannot withstand enough deformation pressure for pumping; therefore, we trade off the thickness of 1 mm to assure a high flow rate and reliability simultaneously.

Figure 3c shows the pressure variations during the working cycles of the soft pump. After 15 s of heating, the ejecting

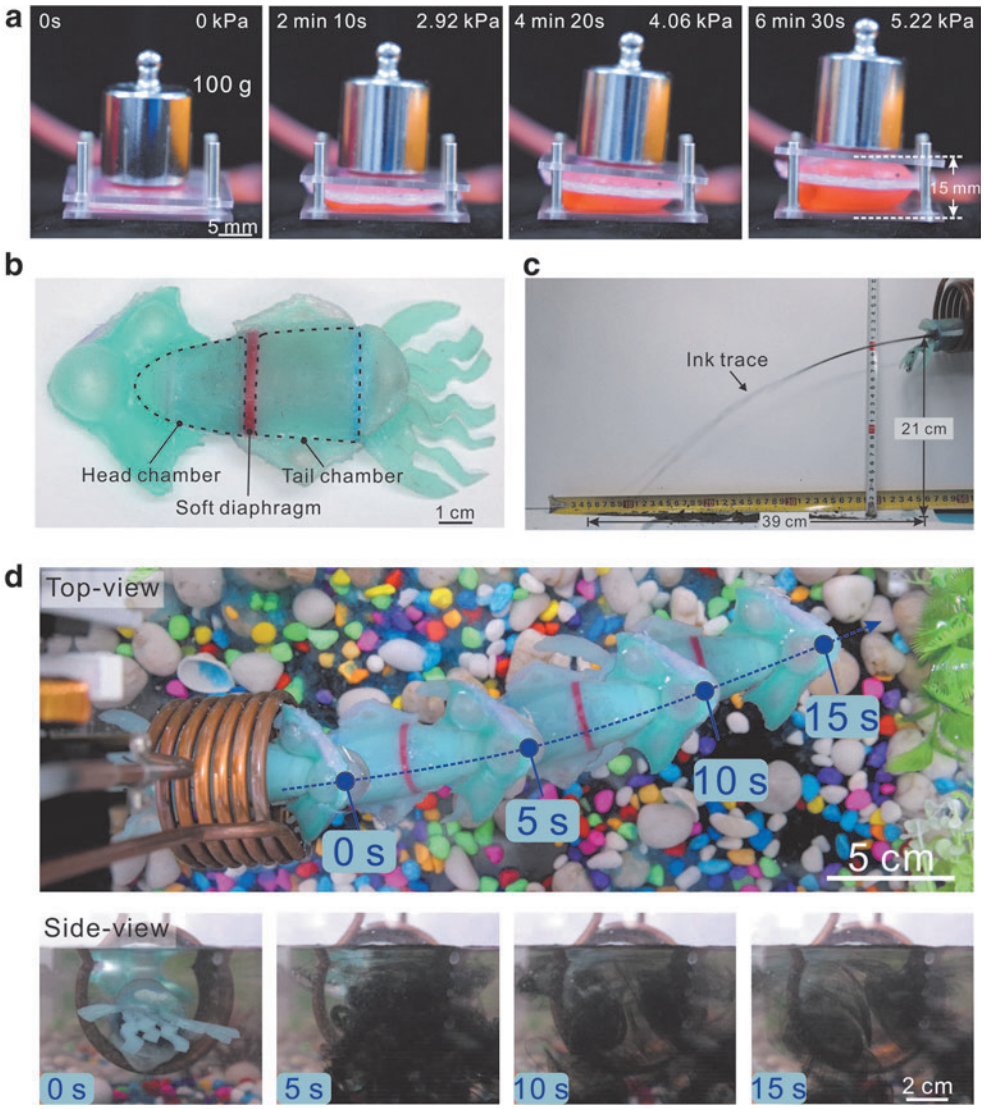

FIG. 4. Demonstrations. **(a)** Time-lapse of the 100 g weight lifted by a soft balloon. The pressure was measured in the soft balloon. **(b)** Image of a soft robotic squid. **(c)** Picture showing the spurt out of black ink. **(d)** Time-lapse of the untethered swimming motion under the water of the squid-like soft robot.

pressure of the pump gradually intensifies up to $\sim$20 kPa, indicating the maximum pumping pressure of the ECSDP. In the subsequent 45 s of cooling, the high-pressure gas in the chamber condensed to liquid, and the suction pressure increased to $\sim$−3.5 kPa. The pressure variation of the soft pump remained constant during three cycling tests.

Theoretically, the longer time the working fluid is heated, the more time it needs to cool down. To balance the heating and cooling process, our experiments show that setting the heating time at 5 s and the cooling time at 30 s can reach a fast flow rate and short interval time. Since the phase of the working fluid needs time to transform, a single ECSDP cannot continuously pump fluid (Fig. 3d). Fortunately, this problem can be compromised by combining multisoft pumps as an associate system to reduce the interval time. In three-pump and six-pump combinations, the interval between two adjacent pumps can be reduced to 7 and 1 s, respectively, using intermittent cooling. When the number of pump combinations rises, the fluid discharge process gradually becomes continuous (Supplementary Video S1). Theoretically, the interval time can be additionally minimized by utilizing extra pump combinations.

We compared the characteristics of ECSDP with previous soft pumps.[18,46–51] The ECSDP with a volume of 2.8 cm^3 can generate a maximum pressure of $\sim$20 kPa and a maximum flow rate of 14.4 mL/min. As in Figure 3e, the ECSDP unifies the unique properties of miniature dimensions and powerful output, enabling a large specific flow rate (5.14 mL/[min·cm^3]) and high specific pressure (7.14 kPa/cm^3). Even though the specific flow rate of the ECSDP is lower than the DEA pump[49] and EHD pump[18] is affected by the working fluid's phase-transition speed, the ECSDP can generate the highest specific pressure among all other listed soft pumps and achieve $\sim$3 times the second-highest record[18] (details in Supplementary Table S1). In addition, compared with the human heart, the ECSDP can provide much higher specific pressure. Hence, the ECSDP can generate a powerful working pressure and flow rate together with superior flexibility and accurate remoting control. More importantly, ECSDP overcomes the issues of complex structure, unembedding, limited working media, and insufficient output capacity of existing soft actuation techniques.

Demonstrations

Several demonstrations of the ECSDP for soft robots are shown in Figure 4. In Figure 4a, time-lapse images show that a 100 g weight was lifted by a soft balloon, which is hydraulically actuated by an ECSDP weighing only $\sim$5 g. The ECSDP had presupposed heating time for 5 s and cooling time for 30 s. The weight was gradually lifted as the ECSDP provided a high output pressure. After 6 min 30 s, the weight was lifted to 15 mm height, and the pressure inner the soft balloon was up to 5.22 kPa (Supplementary Video S2).

The ECSDP can be well integrated into a squid-like soft robot (Fig. 4b). The illustration shows that the soft robotic fish can jet black ink out the tail by inductively heating (Fig. 1b). To investigate the speed of jet flow, we heated the soft robotic fish in a coil to jet the ink horizontally. According to the trace of the ink, the maximum flow rate of the jet flow was calculated as $\sim$1.9 m/s (details in Supplementary Note 2). The soft squid robot can swim in the water under strong jet propulsion (Fig. 4d). After inductive heating started at 0 s, the liquid–gas transition of the working fluid started to occur in the head chamber. Then, the soft robot gradually floated up and ejected black ink backward (Supplementary Video S3). Mimicking the same pulse-jet strategy of actual squids, the soft squid robot swam forward at $\sim$20 mm/s speed (top-view, Fig. 4d) and gradually disappeared with the black ink diffusion (side-view, Fig. 4d).

Conclusion

In this study, inspired by the unique actuation system of squids, we establish an ECSDP to achieve an untethered, fully soft, and powerful actuation system. The ECSDP offers several favorable characteristics: fully soft architecture, remote control, high-pressure output, lightweight design, miniaturized dimensions, and customizable applications. In addition, the ECSDP can pump diverse media (fluid and gas) with a broad viscosity range, and its flow rates can be easily controlled by adjusting the magnetic field. Compared with other soft pumps and the human heart, the ECSDP can provide the highest specific pressure (7.14 kPa/cm^3). Two demonstrations of ECSDPs have been presented to explore their potential fully. A miniaturized ECSDP can lift $\sim$20 times weight. Moreover, the ECSDP can be compatibly embedded into a bionic soft robotic squid to achieve untethered swimming by pulse jetting. Our approach offers a new solution for designing high execution power and portable untethered soft robots.

Authors' Contributions

Z.W. and Q.J. conceived the concept. Q.J., Z.H., K.W., and W.W. conducted the experiments and processed data. Q.J., K.W., and Z.W. drafted the article. Q.J., Z.H., K.W., W.W., S.Z., and Z.W. analyzed the data and interpreted the results. S.Z. and Z.W. directed the project. All authors commented on the article.

Author Disclosure Statement

No competing financial interests exist.

Funding Information

This work was supported by the National Natural Science Foundation of China (52188102). S.Z. thanks the support from the China Postdoctoral Science Foundation (2021M70 1311).

Supplementary Material

Supplementary Note 1
Supplementary Note 2
Supplementary Figure S1
Supplementary Figure S2
Supplementary Figure S3
Supplementary Figure S4
Supplementary Figure S5
Supplementary Figure S6
Supplementary Figure S7
Supplementary Table S1
Supplementary Video S1
Supplementary Video S2
Supplementary Video S3

References

1. Kim W, Byun J, Kim JK, et al. Bioinspired dual-morphing stretchable origami. Sci Robot 2019;4(36):1–11; doi: 10.1126/scirobotics.aay3493
2. Yang Y, Vella K, Holmes DP. Grasping with Kirigami shells. Sci Robot 2021;6(54):eadb6426; doi: 10.1126/scirobotics.abd6426
3. Lin Y, Zhang C, Tang W, et al. A bioinspired stress-response strategy for high-speed soft grippers. Adv Sci 2021;8(21):1–8; doi: 10.1002/advs.202102539
4. Wang L, Zheng D, Harker P, et al. Evolutionary design of magnetic soft continuum robots. Proc Natl Acad Sci 2021; 118(21):e2021922118; doi: 10.1073/pnas.2021922118
5. Zhou C, Yang Y, Wang J, et al. Ferromagnetic soft catheter robots for minimally invasive bioprinting. Nat Commun 2021;12(1):5072; doi: 10.1038/s41467-021-25386-w
6. Lu H, Zhang M, Yang Y, et al. A bioinspired multilegged soft millirobot that functions in both dry and wet conditions. Nat Commun 2018;9(1):3944; doi: 10.1038/s41467-018-06491-9
7. Alapan Y, Yasa O, Schauer O, et al. Soft erythrocyte-based bacterial microswimmers for cargo delivery. Sci Robot 2018;3(17):eaar4423; doi: 10.1126/SCIROBOTICS.AAR4423
8. Wang B, Chan KF, Yuan K, et al. Endoscopy-assisted magnetic navigation of biohybrid soft microrobots with rapid endoluminal delivery and imaging. Sci Robot 2021; 6(52):eabd2813; doi: 10.1126/SCIROBOTICS.ABD2813
9. Heng W, Solomon S, Gao W. Flexible electronics and devices as human–machine interfaces for medical robotics. Adv Mater 2022;34:2107902; doi: 10.1002/adma.202107902
10. Bai H, Li S, Barreiros J, et al. Stretchable distributed fiber-optic sensors. Science 2020;370(6518):848–852; doi: 10.1126/science.aba5504
11. Polygerinos P, Correll N, Morin SA, et al. Soft robotics: Review of fluid-driven intrinsically soft devices; Manufacturing, sensing, control, and applications in human-robot interaction. Adv Eng Mater 2017;19(12):1700016; doi: 10.1002/adem.201700016
12. Rich SI, Wood RJ, Majidi C. Untethered soft robotics. Nat Electron 2018;1(2):102–112; doi: 10.1038/s41928-018-0024-1
13. Drotman D, Jadhav S, Sharp D, et al. Electronics-free pneumatic circuits for controlling soft-legged robots. Sci Robot 2021;6(51):eaay2627; doi: 10.1126/scirobotics.aay2627
14. Tolley MT, Shepherd RF, Mosadegh B, et al. A resilient, untethered soft robot. Soft Robot 2014;1(3):213–223; doi: 10.1089/soro.2014.0008
15. Bartlett NW, Tolley MT, Overvelde JTB, et al. A 3D-printed, functionally graded soft robot powered by combustion. Science 2015;349(6244):161–165; doi: 10.1126/science.aab0129
16. Li G, Chen X, Zhou F, et al. Self-powered soft robot in the Mariana Trench. Nature 2021;591(7848):66–71; doi: 10.1038/s41586-020-03153-z
17. Li T, Li G, Liang Y, et al. Fast-moving soft electronic fish. Sci Adv 2017;3(4):1–8; doi: 10.1126/sciadv.1602045
18. Tang W, Zhang C, Zhong Y, et al. Customizing a self-healing soft pump for robot. Nat Commun 2021;12(1): 2247; doi: 10.1038/s41467-021-22391-x
19. Kim Y, Yuk H, Zhao R, et al. Printing ferromagnetic domains for untethered fast-transforming soft materials. Nature 2018;558(7709):274–279; doi: 10.1038/s41586-018-0185-0
20. Ke X, Zhang S, Chai Z, et al. Flexible discretely-magnetized configurable soft robots via laser-tuned selective transfer printing of anisotropic ferromagnetic cells. Mater Today Phys 2021;17:100313; doi: 10.1016/j.mtphys.2020.100313
21. Wani OM, Zeng H, Priimagi A. A light-driven artificial flytrap. Nat Commun 2017;8(May):1–7; doi: 10.1038/ncomms15546
22. Mirvakili SM, Sim D, Hunter IW, et al. Actuation of untethered pneumatic artificial muscles and soft robots using magnetically induced liquid-to-gas phase transitions. Sci Robot 2020;5(41):1–10; doi: 10.1126/SCIROBOTICS.AAZ4239
23. Mirvakili SM, Leroy A, Sim D, et al. Solar-driven soft robots. Adv Sci 2021;8(8):1–7; doi: 10.1002/advs.202004235
24. Yang X, Shang W, Lu H, et al. An agglutinate magnetic spray transforms inanimate objects into millirobots for biomedical applications. Sci Robot 2020;5(48):1–13; doi: 10.1126/scirobotics.abc8191
25. Katzschmann RK, DelPreto J, MacCurdy R, et al. Exploration of underwater life with an acoustically controlled soft robotic fish. Sci Robot 2018;3(16):1–13; doi: 10.1126/SCIROBOTICS.AAR3449
26. Hu W, Lum GZ, Mastrangeli M, et al. Small-scale soft-bodied robot with multimodal locomotion. Nature 2018; 554(7690):81–85; doi: 10.1038/nature25443
27. Li M, Wang Y, Chen A, et al. Flexible magnetic composites for light-controlled actuation and interfaces. Proc Natl Acad Sci U S A 2018;115(32):8119–8124; doi: 10.1073/pnas.1805832115
28. Fan X, Dong X, Karacakol AC, et al. Reconfigurable multifunctional ferrofluid droplet robots. Proc Natl Acad Sci U S A 2020;117(45):27916–27926; doi: 10.1073/pnas.2016388117
29. Umbanhowar PB, Komsuoglu H, Koditschek DE, et al. Phototactic guidance of a tissue-engineered soft-robotic ray. Science 2016;353(6295):158–162; doi: 10.1126/science.aaf4292
30. Yang Y, Liu Y, Shen Y. Plasmonic-assisted graphene oxide films with enhanced photothermal actuation for soft robots. Adv Funct Mater 2020;30(14):1910172; doi: 10.1002/adfm.201910172
31. Li S, Bai H, Liu Z, et al. Digital light processing of liquid crystal elastomers for self-sensing artificial muscles. Sci Adv 2021;7(30):eabg3677; doi: 10.1126/sciadv.abg3677
32. Bartol IK, Krueger PS, Thompson JT, et al. Swimming dynamics and propulsive efficiency of squids throughout ontogeny. Integr Comp Biol 2008;48(6):720–733; doi: 10.1093/icb/icn043
33. Bujard T, Giorgio-Serchi F, Weymouth GD. A resonant squid-inspired robot unlocks biological propulsive efficiency. Sci Robot 2021;6(50):eabd2971; doi: 10.1126/SCIROBOTICS.ABD2971
34. Hu J, Li H, Chen W. A squid-inspired swimming robot using folding of origami. J Eng 2021;2021(10):630–639; doi: 10.1049/tje2.12075
35. Bartlett MD, Kazem N, Powell-Palm MJ, et al. High thermal conductivity in soft elastomers with elongated liquid metal inclusions. Proc Natl Acad Sci U S A 2017; 114(9):2143–2148; doi: 10.1073/pnas.1616377114
36. Wang H, Yao Y, Wang X, et al. Large-magnitude transformable liquid-metal composites. ACS Omega 2019;4(1): 2311–2319; doi: 10.1021/acsomega.8b03466

37. Markvicka EJ, Bartlett MD, Huang X, et al. An autonomously electrically self-healing liquid metal-elastomer composite for robust soft-matter robotics and electronics. Nat Mater 2018;17(7):618–624; doi: 10.1038/s41563-018-0084-7
38. Wissman J, Dickey MD, Majidi C. Field-controlled electrical switch with liquid metal. Adv Sci (Weinh) 2017; 4(12):1700169; doi: 10.1002/advs.201700169
39. Malakooti MH, Kazem N, Yan J, et al. Liquid metal supercooling for low-temperature thermoelectric wearables. Adv Funct Mater 2019;29(45):1–9; doi: 10.1002/adfm.201906098
40. Wang H, Chen S, Yuan B, et al. Liquid metal transformable machines. Accounts Mater Res 2021;2(12):1227–1238; doi: 10.1021/accountsmr.1c00182
41. Wang X, Guo R, Liu J. Liquid metal based soft robotics: Materials, designs, and applications. Adv Mater Technol 2019;4(2):1–15; doi: 10.1002/admt.201800549
42. Li Y, Feng S, Cao S, et al. Printable liquid metal microparticle ink for ultrastretchable electronics. ACS Appl Mater Interfaces 2020;12(45):50852–50859; doi: 10.1021/acsami.0c15084
43. Park S, Baugh N, Shah HK, et al. Ultrastretchable elastic shape memory fibers with electrical conductivity. Adv Sci 2019;6(21):1901579; doi: 10.1002/advs.201901579
44. Wang H, Chen S, Li H, et al. A liquid gripper based on phase transitional metallic ferrofluid. Adv Funct Mater 2021;2100274:1–9; doi: 10.1002/adfm.202100274.
45. Marechal L, Balland P, Lindenroth L, et al. Toward a common framework and database of materials for soft robotics. Soft Robot 2021;8(3):284–297; doi: 10.1089/soro.2019.0115
46. Jang LS, Li YJ, Lin SJ, et al. A stand-alone peristaltic micropump based on piezoelectric actuation. Biomed Microdevices 2007;9(2):185–194; doi: 10.1007/s10544-006-9020-8
47. Van de Pol FCM, Van Lintel HTG, Elwenspoek M, et al. A thermopneumatic micropump based on micro-engineering techniques. Sensors Actuators A Phys 1990;21(1–3):198–202; doi: 10.1016/0924-4247(90)85038-6
48. Stergiopulos C, Vogt D, Tolley MT, et al. A Soft Combustion-Driven Pump for Soft Robots. In: Proceedings of the ASME 2014 Conference on Smart Materials, Adaptive Structures and Intelligent Systems 2014; pp. 1–6; doi: 10.1115/SMASIS20147536
49. Cao C, Gao X, Conn AT. A magnetically coupled dielectric elastomer pump for soft robotics. Adv Mater Technol 2019; 4(8):1–6; doi: 10.1002/admt.201900128
50. Sim WY, Yoon HJ, Jeong OC, et al. A phase-change type micropump with aluminum flap valves. J Micromech Microeng 2003;13(2):286–294; doi: 10.1088/0960-1317/13/2/317
51. Zhou M, Qi Z, Xia Z, et al. Miniaturized soft centrifugal pumps with magnetic levitation for fluid handling. Sci Adv 2021;7(44):1–14; doi: 10.1126/sciadv.abi7203

Address correspondence to:
Shuo Zhang
State Key Laboratory of Digital Manufacturing Equipment and Technology
School of Mechanical Science and Engineering
Huazhong University of Science and Technology
Wuhan 430074
China

E-mail: shuo_zhang@hust.edu.cn

Zhigang Wu
State Key Laboratory of Digital Manufacturing Equipment and Technology
School of Mechanical Science and Engineering
Huazhong University of Science and Technology
Wuhan 430074
China

E-mail: zgwu@hust.edu.cn